



# Acoustic metamaterial absorbers: The path to commercialization



Cite as: Appl. Phys. Lett. **122**, 260504 (2023); doi: [10.1063/5.0147941](https://doi.org/10.1063/5.0147941)

Submitted: 27 February 2023 · Accepted: 12 June 2023 ·

Published Online: 29 June 2023



View Online



Export Citation



CrossMark

Min Yang<sup>1,a)</sup> and Ping Sheng<sup>2,a)</sup>

## AFFILIATIONS

<sup>1</sup>Acoustic Metamaterials Group, Unit 608-610, Data Technology Hub, No. 5 Chun Cheong Street, Tseung Kwan O, New Territories, Hong Kong, China

<sup>2</sup>Institute for Advanced Study, Hong Kong University of Science and Technology, Clear Water Bay, Kowloon, Hong Kong, China

<sup>a)</sup>Authors to whom correspondence should be addressed: [min@metacoust.com](mailto:min@metacoust.com) and [sheng@ust.hk](mailto:sheng@ust.hk)

## ABSTRACT

Acoustic metamaterial represents the synergism between wave physics and designed geometric structures, aimed at novel acoustic properties. For the important functionality of acoustic absorption, metamaterials face the challenges posed by a mature, existing group of absorbing materials that have proven their effectiveness. Can the metamaterials do better? If so, at what price? This article aims to answer these important questions. In particular, it is shown that the critical advantage offered by metamaterial absorbers lies in the tunability of the absorption spectrum to fit the needs of the client, in conjunction with a minimum absorber thickness set by the causal constraint. By overcoming the obstacles set by the mass production cost, acoustic metamaterial absorbers have now entered the commercialization stage. We give three examples of the commercialized applications together with their underlying working principles and conclude with some observations.

© 2023 Author(s). All article content, except where otherwise noted, is licensed under a Creative Commons Attribution (CC BY) license (<http://creativecommons.org/licenses/by/4.0/>). <https://doi.org/10.1063/5.0147941>

## I. INTRODUCTION

Two decades after the initiation of the acoustic metamaterial field, a clear bifurcation is evident: While one direction points to the continued pursuit of novel phenomena,<sup>1-9</sup> mostly through topological structures,<sup>10-13</sup> the other points to practical applications on those problems difficult to resolve through conventional means, with the ultimate goal of commercialization. This article intends to address the latter, in the area of acoustic absorption.

Acoustic noise is still a pervasive problem in the 21st century. This is especially the case for low frequency noise arising from machines, traffic, railroad, airplanes, etc. Such noise can be absorbed by conventional absorbers, but the required material volume often makes their use impractical. This opens an opportunity for metamaterial absorbers. Can metamaterials do better against the array of low-cost conventional acoustic materials such as foam, rock wool, fiberglass wool, etc.? In the past few years, this question has been answered in the affirmative.<sup>14</sup> In this article, we show that metamaterials' customizability enables the maximum absorption allowed by causality for any specific noise, with the minimum absorber thickness. The resulting absorption performance, in the case of mechanical noise and within the confines of limited space, is often far superior to traditional absorbers. On the other hand, the relevant structural scale of

acoustic metamaterial absorbers makes them suitable to be mass-produced by using the molding process with a diverse selection of materials, e.g., metal for high-temperature applications, plastic or paper for lightweight applications, ceramics for applications requiring high hardness, etc. The acoustic absorption functionality of the metamaterial absorbers is independent from the materials they are made.

In what follows, we present in Sec. II the two different paths to achieve high acoustic absorption and their relevant structural scales. This is followed by a succinct presentation of the theoretical basis for the metamaterials design and its implementation scheme in Sec. III. A practical example to illustrate the effectiveness of the design approach is given in Sec. IV, together with the actual experimental results. In Sec. V, we give three examples of commercialized applications. We conclude in Sec. VI with some observations.

## II. ABSORPTION BY TRADITIONAL OR METAMATERIAL ABSORBERS, AND THEIR RELEVANT STRUCTURAL SCALES

In the field of optics, a critical characteristic that sets metamaterials apart from traditional materials is that their performance is achieved through their structure, rather than their chemical composition. However, traditional porous materials in acoustics also

demonstrate absorption properties that are primarily a result of their porous structure. Consequently, an essential question arises: what distinguishes the structural characteristics of acoustic metamaterials from those of traditional porous materials? Addressing this question will also reveal the most significant advantages of using acoustic metamaterials in various applications.

### A. Porous absorbers

Traditional porous materials, such as foam, rock wool, and fiberglass wool, absorb sound through the friction of air molecules at an interfacial layer between air and the solid skeleton denoted the viscous boundary layer,<sup>14,15</sup> in which the molecular displacement velocity of air exhibits a monotonic gradient field [Fig. 1(a)] over a length scale given by  $\delta = \sqrt{\frac{2\nu}{2\pi f}}$ , with  $\nu = 1.5 \times 10^{-5}$  m<sup>2</sup>/s being the kinematic viscosity of air and  $f$  the sound frequency. Accordingly, a natural way

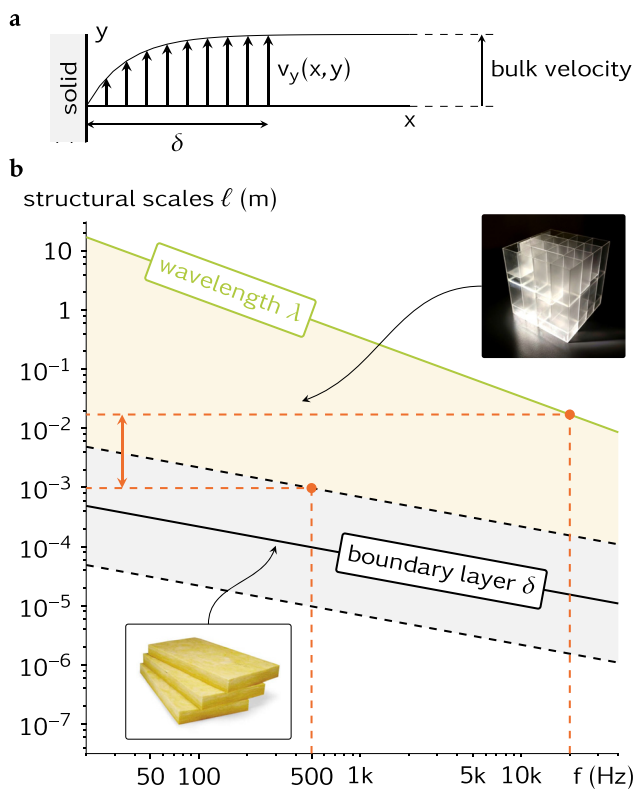


**FIG. 1.** Relevant spatial scales of acoustic porous materials and metamaterials. (a) Air molecules' velocity field near a solid surface. Here, the  $y$  axis denotes the air molecules' displacement velocity. The monotonically increasing velocity region defines the scale  $\delta$  of the viscous boundary layer. (b) The black line represents the boundary layer thickness as a function of frequency. The green line denotes the wavelength. The gray-shaded region indicates the structural scales of acoustic porous absorbers. They deviate from  $\delta$  by less than an order of magnitude. The yellow-shaded region denotes the structural scales of acoustic metamaterials. For metamaterial absorbers functioning in the frequency range of 500–20 000 Hz [the one shown in Fig. 3(b)], the structural scales range from millimeters to several centimeters (delineated by red dashed lines). Two insets are examples of mass-produced acoustic metamaterials (top right) and glass fiber wool (bottom left).

to improve the sound absorption efficiency is to increase the solid/air interfacial area so as to enhance the dissipation efficiency per unit volume. Efficient porous absorbers tend to have porosities close to 1; with an average pore size,  $l$ , on the order of  $\delta$  [the gray region in Fig. 1(b)], so as to maximize the absorption within the given volume.<sup>15</sup> The porous absorbers inherently have a low quality factor, with a broadband absorption spectrum. It should be noted, however, that the dissipation coefficient of a porous absorber should not be too high; otherwise, the impedance mismatch, at the interface between air and the absorber, can prevent sound waves from entering the material.<sup>14</sup> Therefore, impedance mismatch is always a competing consideration for a porous absorber. As impedance is an important parameter for an absorber, its definition and implications are detailed later, in Sec. III.

### B. Metamaterials take a different path to high absorption

High dissipation coefficient is not the only way to increase absorption. Energy absorption density is the product of a material's dissipation coefficient with the local sound energy density; hence, higher energy density can also increase absorption. Metamaterial absorbers essentially take this alternative path. By designing local resonances<sup>1,8</sup> to increase the local energy density, acoustic metamaterials require only weak material dissipation coefficient, with structural scales  $l \gg \delta$ , so that the absorber can attain impedance-match with air, to achieve almost 100% absorption.<sup>14,16–27</sup> As metamaterials' locally resonant structures are generally subwavelength in nature with  $l < \lambda = \frac{c}{f}$ , where  $c = 343$  m/s is the speed of sound in air, the structural scales fall in the yellow-shaded region shown in Fig. 1(b). However, metamaterial absorber's low-dissipation and subwavelength nature dictate its absorption to always display sparse and narrow-frequency peaks with high quality factors.<sup>14</sup> Even though narrow-frequency band absorption can be meaningful in some special occasions, most practical applications still require broadband noise absorption capability. In order to compensate for this inherent defect of metamaterial absorbers, it is natural to pursue the strategy of integrating multiple units, each resonant at a different frequency, so as to broaden the absorption frequency spectrum.<sup>28–57</sup> Such strategies share the common element of leveraging a multi-modal system, each mode having low dissipation, to achieve broadband effective absorption. In Fig. 2, we illustrate some examples that utilized this mechanism.

It turns out that there exists an optimal integration scheme for attaining broadband and tunable absorption spectrum that can surpass the performance of traditional acoustic absorbers in defined applications. Moreover, one can inverse-design the metamaterial absorber to have a target absorption spectrum, in conjunction with a minimum sample thickness as dictated by the law of nature. In terms of commercialization, this high degree of customizability brings about a paradigm shift in many areas of acoustic applications. We detail this design scheme by starting from the fundamental limitation imposed by causality on wave absorption as follows.

## III. THEORETICAL BASIS

### A. Absorption optimization with the causality constraint

As time can only proceed in one direction, i.e., toward the future, the law of causality states that what happens on an absorber at any instant of time can only depend on what happened before that instant,

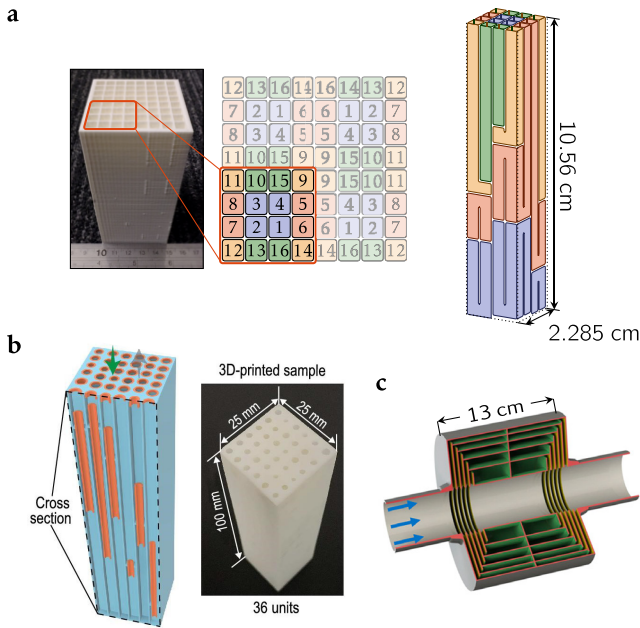


**FIG. 2.** Examples of broadband acoustic metamaterials and their geometric scales. Both acoustic Fabry-Pérot resonators shown in (a) and Helmholtz resonators shown in (b) and (c) of similar geometric dimensions can provide similar absorptance for normally incident sounds. In ventilation system shown in (c), air passes through the central cylindrical channel. Sound absorption structures surround the central channel. The figures in (a) are adapted from Ref. 28. The figures in (b) are reproduced with permission from Zhou *et al.*, Natl. Sci. Rev. 9, nwab171 (2022). Copyright 2022 Oxford Academic Publishing. The figures in (c) are reproduced with permission from Nguyen *et al.*, Appl. Phys. Lett. 117, 134103 (2020). Copyright 2020 AIP Publishing.

not on what will happen in the future. Mathematically, Fourier transform teaches us that time and frequency are conjugate variables. The imposition of causality in the time domain, i.e., the asymmetry in time, has profound implications for the material properties in the frequency domain. In particular, during the 1920s, Hans Kramers and Ralph Kronig independently derived the famous Kramers-Kronig relation between the real and imaginary parts of the dielectric function.<sup>58</sup> Another consequence of the causality law is the Bode-Fano bound for network matching,<sup>59,60</sup> and more recent studies also revealed a relationship between an absorber’s thickness and its absorption spectrum, expressible as an inequality,<sup>14,61,62</sup>

$$d \geq -\frac{1}{4\pi^2} \int_0^\infty \ln[1 - A(\lambda)] d\lambda = \tau, \quad (1)$$

where  $d$  is the sample thickness,  $A(\lambda)$  is the ratio of the absorbed energy to the normally incident energy at wavelength  $\lambda$ . One important conclusion from Eq. (1) is that perfect absorber like blackbody cannot exist because  $A = 1$  in any finite bandwidth will cause the integral to diverge. The causal inequality also emphasizes the importance of sample thickness as a “resource” for wave absorption. For a given  $\tau$ , enhanced absorption in one frequency band is usually at the expense of decreased absorption in others—one cannot increase absorption without any cost. Therefore, for a specific signal energy spectrum,  $S(\lambda)$ , any redundant absorption outside the signal’s frequency range is

a waste, and its maximum absorption should correspond to a material-independent absorption spectrum determined only by the thickness of the absorber. We denote this  $A(\lambda)$  the causally optimal broadband absorption (COBA) spectrum for the incident signal, which represents an absorber’s upper limit allowed by the law of causality. Mathematically, COBA corresponds to the maximum in the total absorption defined by  $E[A(\lambda)] \equiv \int_0^\infty S(\lambda)A(\lambda)d\lambda$  subject to the constraints of Eq. (1) and a given value of  $d$ . Here,  $S(\lambda)$  is in the unit of power per unit wavelength.

To find the solution of this optimization problem, we introduce a Lagrange multiplier  $\mu$  to form the functional,

$$E_\mu[A(\lambda)] \equiv \int_0^\infty S(\lambda)A(\lambda)d\lambda - \mu \left\{ \frac{-1}{4\pi^2} \int_0^\infty \ln[1 - A(\lambda)]d\lambda - d \right\}. \quad (2a)$$

According to the Karush-Kuhn-Tucker condition,<sup>63</sup> the optimum in  $E_\mu[A(\lambda)]$  requires the variation  $\frac{\delta E_\mu}{\delta A} = 0$ , with

$$\begin{cases} \frac{-1}{4\pi^2} \int_0^\infty \ln(1 - A)d\lambda - d \leq 0 \\ \mu > 0 \\ \mu \left[ \frac{-1}{4\pi^2} \int_0^\infty \ln(1 - A)d\lambda - d \right] = 0. \end{cases} \quad (2b)$$

The theoretical maximum absorption is given by  $E_{\max} = \int_0^\infty S(\lambda)A_{\text{COBA}}(\lambda)d\lambda$ , with  $A_{\text{COBA}}$  obtained from the condition  $\frac{\delta E_\mu}{\delta A} = 0$  as

$$A_{\text{COBA}}(\lambda) = \begin{cases} 1 - \frac{\mu}{4\pi^2} \frac{1}{S(\lambda)} & \frac{\mu}{4\pi^2} \frac{1}{S(\lambda)} \leq 1 \\ 0 & \frac{\mu}{4\pi^2} \frac{1}{S(\lambda)} > 1 \end{cases}, \quad (3a)$$

where the second condition ensures  $A \geq 0$  so as to preserve the conservation of energy, and the Lagrange multiplier  $\mu$  takes the value which satisfies the condition

$$-\frac{1}{4\pi^2} \int_0^\infty \ln[1 - A_{\text{COBA}}(\lambda)]d\lambda = d. \quad (3b)$$

This can be done by substituting the solution of Eq. (3a) into the integral of Eq. (3b). For a given  $d$  and a known incident spectrum  $S(\lambda)$ , the maximum absorption can be explicitly evaluated.

According to Eq. (3), each noise signal  $S(\lambda)$  has a unique COBA for a given thickness  $d$ . The realization of COBA, or the design that targets it, can mean the optimal absorber performance at the minimum thickness.

### B. Implementation strategy to attain the optimal absorption spectrum

According to the scheme presented in Ref. 28, metamaterial’s absorption is given by  $A = 1 - |(Z - \rho c)/(Z + \rho c)|^2$ , where  $\rho = 1.2 \text{ kg/m}^3$  is the air density and  $Z = p/v$  denotes the surface impedance. Here,  $p$  is the pressure modulation of sound and  $v$  is the associated molecular displacement velocity. For a resonator array facing sound in parallel [as shown in the inset of Fig. 3(b)], its surface impedance can be expressed in terms of a summation of Lorentzians,

$$Z(\omega) = \frac{i}{\omega} \left( \frac{\phi}{N} \sum_{n=1}^N \frac{r_n}{\omega_n^2 - \omega^2 - i\omega\beta} \right)^{-1}$$

$$= \frac{i}{\omega} \left\{ \frac{\phi}{N} \sum_{n=1}^N \left[ \frac{r_n(\omega_n^2 - \omega^2)}{\omega^2\beta^2 + (\omega_n^2 - \omega^2)^2} + \frac{ir_n\omega\beta}{\omega^2\beta^2 + (\omega_n^2 - \omega^2)^2} \right] \right\}^{-1},$$

in which  $\beta$  is the damping coefficient,  $\omega = 2\pi f$  is the angular frequency of the incident source,  $r_n$  and  $\omega_n$  are the resonance strength and angular frequency of the  $n$ th resonator, respectively,  $N$  denotes the total number of resonators, and the surface porosity  $\phi$  is the fraction of resonators' total opening area to the area exposed to the incident sound. For simplicity, here, we ignore the higher-order modes of the resonators, which can be corrected by a more exact treatment.<sup>28</sup>

As the first term in the aforementioned summation changes sign from negative to positive around each resonance frequency, the summation of all the modes tends to cancel, leading to a negligible net result. In contrast, since the second term of the summation is always positive, the contributions of all modes are cumulatively added to each other, resulting in a relatively large value. Therefore, we can define a modal density,  $\mathcal{N}_d(\omega) \equiv dn/d\omega$ , to convert the summation into an integral and approximate the impedance in terms of a real-valued integral,

$$Z(\omega) \simeq \frac{1}{\omega} \left[ \frac{\phi}{N} \int_{\omega_1}^{\omega_N} \frac{r(x)\omega\beta}{\omega^2\beta^2 + (x^2 - \omega^2)^2} \mathcal{N}_d(x) dx \right]^{-1},$$

in which  $\omega_1(\omega_N)$  is the frequency of the 1st ( $n$ th) (lowest frequency) resonance. As mentioned earlier, metamaterials inherently have high Q factors that imply a small  $\beta$ . That means we can further simplify the impedance expression as

$$\lim_{\beta \rightarrow 0} Z(\omega) = \frac{2N}{\omega\pi\phi} \left[ \int_{\omega_1}^{\omega_N} \frac{r(x)}{x} \delta(\omega - x) \mathcal{N}_d(x) dx \right]^{-1}$$

$$= \frac{2N}{\pi\phi} \frac{1}{\mathcal{N}_d(\omega)r(\omega)}. \tag{4}$$

Equation (4) conveys an important message: Metamaterials can adjust the impedance and thereby enable customized absorption by adjusting the modal density,  $\mathcal{N}_d(\omega)$ . Specifically, for a target absorption spectrum  $A(\omega)$ , as the relevant real  $Z = \rho c(2 + 2\sqrt{1 - A} - A)/A$ , the suitable  $\mathcal{N}_d(\omega)$  is given by

$$\mathcal{N}_d(\omega) = \frac{2N}{\pi\phi\rho c} \frac{A(\omega)/r(\omega)}{2 + 2\sqrt{1 - A(\omega)} - A(\omega)}, \tag{5}$$

where the strength function,  $r(\omega)$ , depends on the specific type of resonator, and the surface porosity,  $\phi$ , is determined by the normalization condition,  $\int_{\omega_1}^{\omega_N} \mathcal{N}_d(\omega) d\omega = N$ ,

$$\phi = \frac{2}{\pi\rho c} \int_{\omega_1}^{\omega_N} \frac{A(\omega)/r(\omega)}{2 + 2\sqrt{1 - A(\omega)} - A(\omega)} d\omega.$$

#### IV. AN ILLUSTRATIVE EXAMPLE

##### A. Optimal absorption spectrum for the transformer noise

To visualize the consequences of COBA with an example, we optimize the absorption of the noise from an electrical transformer

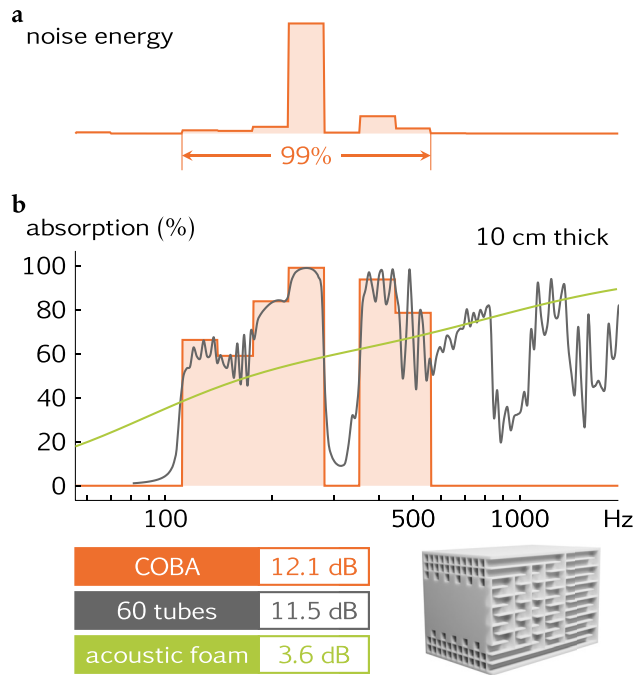


**FIG. 3.** Customized absorption by acoustic metamaterial for the electrical transformer noise. (a) The noise spectrum of a large electrical transformer. About 99% of the noise energy is concentrated between 110 and 560 Hz. (b) The red line is the causally optimal broad absorption (COBA) of this noise spectrum under the thickness constraint of 10 cm. It suppresses the reflection by 12.1 dB through absorption and represents the maximum allowed by causality. Targeting this COBA, an acoustic metamaterial comprising 60 FP resonators is shown to attain the reflection loss of 11.5 dB (black curve) with the same 10 cm thickness. Comparatively, a 10 cm-thick acoustic foam can only provide a reflection loss of about 3.6 dB (green curve). The right-bottom inset shows a photo image of the acoustic metamaterial unit.

with a given thickness of the absorption panel. Figure 3(a) shows a large transformer's noise measured in one-third octave bands, in which 99% of the energy is concentrated in the frequency range from 110 to 560 Hz. If we constrain the absorbing panel thickness to  $\tau = 10$  cm, Eq. (3) gives a COBA solution shown in Fig. 3(b) by the red line. The relevant  $E_{\max}/\int_0^{\infty} S d\lambda = 93.8\%$ , which is equivalent to 12.1 dB in reflection loss [defined as  $-10\log_{10}(1 - E/\int_0^{\infty} S d\lambda)$ ]. In contrast, due to the wasted absorption capacity at lower and higher frequencies [green line in Fig. 3(b)], the traditional acoustic foam with the same 10 cm thickness can only reach the absorption efficiency of 56% (3.6 dB in reflection loss).

##### B. Experimental implementation and comparison with prediction

To test the effectiveness of the design and implement the scheme presented earlier, we have designed the metamaterials panel to realize the COBA for the transformer noise example, with a sample thickness of 10 cm. We utilized quarter-wavelength tubes, i.e., the Fabry-Pérot (FP) resonators, as the fundamental units and adjusted their lengths to design the resonances to be distributed in accordance with Eq. (5). As shown in the inset to Fig. 3(b), a prototype was 3D printed, comprising

60 folded tubes in a compact  $9 \times 9 \times 10 \text{ cm}^3$  maze-like structure, which serves as the functional unit of a flat absorbing panel. In the laboratory impedance tube measurements, it exhibited an absorption spectrum delineated by the black curve in Fig. 3(b). It can be seen that the experimentally measured result, while highly undulating in character, follows closely the COBA solution in the frequency range from 110 to 560 Hz, where the noise energy is concentrated. Its total reflection loss is 11.5 dB, only 0.6 dB lower than COBA and much higher than that of the traditional acoustic foam. The discrepancy with COBA arises mainly from the unavoidable higher-order modes of the FP tubes which absorb sound higher than 560 Hz. However, the higher frequency absorption contributes only a very small fraction to the causal integral of Eq. (1).

The aforementioned example shows that the absorption performance of customized COBA is often far better than that of traditional porous materials, especially when the noise has a large low frequency component. This advantage is the cornerstone for the commercialization of acoustic metamaterials. However, the intricate structures of the metamaterial absorbers usually pose a challenge in mass production. While the flexibility of 3D printing makes it ideal for prototyping and testing,<sup>64,65</sup> the existing 3D printing technology still faces the challenges of production efficiency and yield rate in mass production. Fortunately, because the sound wavelengths are not very small for audible acoustics (20–20 000 Hz) as shown in Fig. 1(b), acoustic metamaterial's structural scales are usually on the order of millimeters to centimeters—exactly in the range of traditional mold production process, which is efficient, reliable, and suitable for mass production. Based on this production process, we have witnessed the launch of many successful commercial acoustic metamaterial products in recent years.

## V. APPLICATIONS

### A. Speakers

One typical example of commercial application is in high fidelity speakers. The sound produced by a speaker comes from the vibration of its diaphragm [the black dome in Fig. 4(a)]. However, its front (blue) and back (red) sound pressures are opposite in phase and can cancel each other in the far field if there is no back enclosure. Therefore, traditional loudspeakers usually place an enclosure behind the diaphragm to block this interference effect and enhance the far-field radiation.

However, since the back cavity still produces reflected waves that can cancel the sound in the front at some specific frequencies, traditionally acoustic sponge was added to suppress the reflected waves, for ensuring speaker's sound efficiency. Acoustic metamaterials can completely replace such absorbing material and provide better results. Furthermore, since the reflection effect of the rear cavity directly affects the frequency response of the speaker diaphragm itself, the customized characteristics of metamaterial can also mean a new way to adjust speaker's sound quality; i.e., by designing the absorption efficiency at different frequencies, one can adjust speaker's sound accordingly, for achieving the desired timbres.

Figure 4(a) shows a metamaterial absorber designed for a mid-high frequency loudspeaker. The absorber is located at the rear end of the speaker and is connected to the space behind the diaphragm via an air duct. The metamaterial consists of 30 tubes of varying lengths wound in two layers to form a disk, operating at frequencies ranging

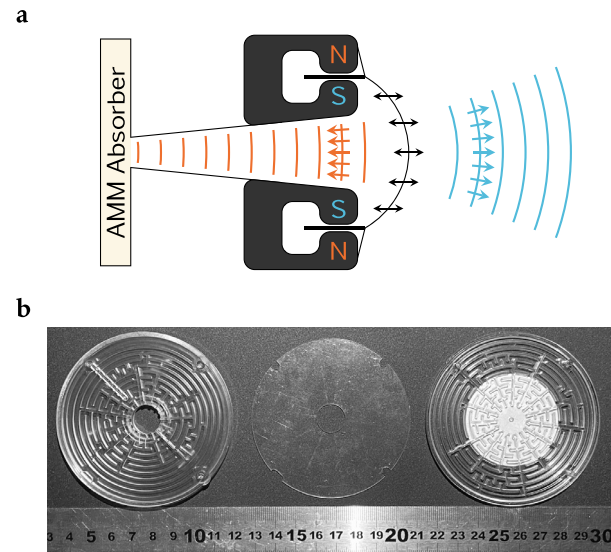


**FIG. 4.** Acoustic metamaterial (AMM) absorber for mitigating the spurious sound from the loudspeaker. (a) Acoustic metamaterial can be used at the back of the speaker driver to absorb the backward sound (indicated by red), generated by the diaphragm (black dome). The customized absorption of the backward sound can tune and improve the quality of forward sound (blue). (b) The relevant metamaterial product was made with three injection-molded parts. The overall thickness is 11 mm. Its fine scale is on the order of millimeters.

from 500 Hz to 20 kHz. According to Fig. 1(b), in this working frequency band, the boundary layer at 500 Hz is thickest at around  $100 \mu\text{m}$ , while the shortest acoustic wavelength is approximately 10 mm at 20 kHz. Therefore, the reasonable size range for the fine structures of the metamaterial should be 1 mm (10 times the thickness of the boundary layer) to 10 mm, meeting the precision of traditional injection molding processes. As such, the final product comprises three injection-molded parts as shown in Fig. 4(b). For the specific acoustic improvements conferred by the metamaterial absorber, please refer to Ref. 66.

### B. Outdoor sound insulation panels

The mold-based production process has led to the possibility of large-scale mass production of metamaterials, which makes possible the applications not only limited to small devices but can also be extended to large-scale scenarios such as mechanical noise reduction that requires large noise absorption panels. The noise of large machineries often has a distinct spectral signature, which gives an inherent advantage to customizable metamaterials. The photo in Fig. 5(a) shows a metamaterial noise reduction facility installed at Kai Tak, Hong Kong. On top of each residential building, ventilated sound-absorbing units [Fig. 5(b)], comprising acoustic metamaterial panels, form walls and ceilings enclosing the building's mechanical systems, such as water pumps, chillers, and fans [Fig. 5(c)]. While absorbing noise, these silencers can also play the role of ventilation, heat dissipation, and equipment protection. A total of more than 5000 square meters of metamaterial panels were used throughout the project indicated in Fig. 5. Each panel surface is covered with perforated metal plates to protect the internal structures from the outdoor environment.

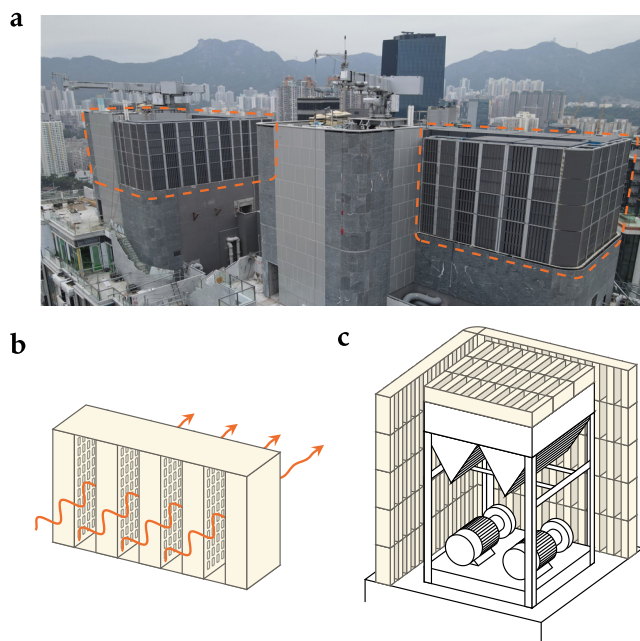


**FIG. 5.** Large-scale outdoor application of mass-produced metamaterials. (a) Photograph of the metamaterial noise reduction facility (marked by the red dashed boxes) installed on top of residential buildings located in Kai Tak, Hong Kong. (b) Schematic drawing of the ventilated silencer made of arrays of metamaterials absorbing panels. Each structured metamaterial panel is covered by the perforated metal plate, to protect it from the outdoor environment. (c) The silencers formed the acoustic fence and ceiling that enclose the machineries (pumps and chillers) on the roof. In this case, the metamaterial absorbers were customized to target an average noise spectrum that originates from the different devices.

To achieve sufficiently high levels of noise reduction within a restricted thickness, the metamaterial panels described here have all been specifically designed in accordance with the noise spectrum of the machine on site, as detailed in Secs. III and IV. This is in contrast to the general broadband ventilation silencers like those described in Refs. 40–42 and 46. However, in such large-scale applications, versatility is also critical for cost control.

Therefore, in customizing the metamaterials, the target noise spectrum is not that of a particular machine but rather the average noise spectra of the various devices:  $S(\lambda) = \sum_n a_n S_n(\lambda) / \sum_n a_n$ , where  $S_n(\lambda)$  denotes the noise spectrum of different machines and the corresponding weight  $a_n$  is determined by the number of machines. About 90% of the noise energy in  $S(\lambda)$  lies in the frequency range of 200–2000 Hz. The relevant metamaterial treatment reduces the mechanical noise to a level of less than 55 dB, measured at 1.5 m on the outside of the metamaterial enclosure, from a level of 68 dB without the enclosure. It should be noted that in contrast to a sound-blocking enclosure, an absorbing enclosure reduces not only the noise outside but also the sound intensity inside the enclosure.

### C. Anechoic chamber

In addition to realizing COBA, customized broadband absorption also has exceptional value in many other scenarios. An interesting

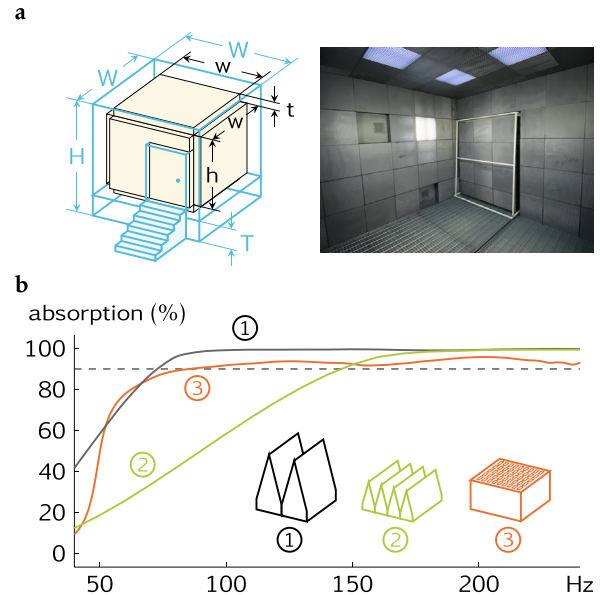


**FIG. 6.** Customized acoustic metamaterial enables anechoic chambers in small spaces. (a) The six inner sides of an anechoic chamber, comprising  $t = 40$  cm thick metamaterial panels (colored). The inner dimensions of the chamber are  $w = 2.74$  and  $h = 2.47$  m. The outer dimensions are  $W = H = 4$  m. A damping platform has the thickness of  $T = 50$  cm. The inset is a photograph of the interior of the anechoic chamber. (b) The black curve is the absorption of an 80 cm thick wedge sponge, plotted as a function of frequency (IAC 100 Hz Metadyne® LF Wedge), while the green curve is the estimation for a wedge scaled down by half (40 cm thick) using the same material. The red curve represents the absorption of the metamaterial panel used in (a), which is 40 cm in thickness. The black dashed line indicates 10 dB reflection loss. The reflection loss for the metamaterial panel exceeds 10 dB above 85 Hz.

example is the anechoic chamber, shown in Fig. 6(a) with a schematic illustration of its geometry on the left panel, and an actual photo of the inside chamber on the right panel, where the six sides are tiled with metamaterial panels.

Traditional anechoic chambers use wedge sponge (or rock wool) as the absorptive material to achieve a high and flat absorption spectrum. However, according to Eq. (1), this necessarily implies a substantial thickness. In particular, for a wedge sponge with a cutoff frequency of 100 Hz as shown in Fig. 6(b), the thickness is approximately 80 cm. Therefore, by taking the dimensions illustrated in the left panel of Fig. 6(a), if the anechoic chamber is to be built in a space of  $400 \times 400 \times 400$  cm<sup>3</sup> (outside dimensions), with a 23 cm sound insulation layer and a 50 cm vibration damping platform at the bottom, the interior space is only a cuboid with a length and width of 194 cm and a height of 167 cm, which is not very suitable for everyday use.

If we scale the wedge down by half to 40 cm thick, the internal space of the chamber will increase to a usable size of  $274 \times 274 \times 247$  cm<sup>3</sup>. However, what about the corresponding absorption? Suppose we use the same sponge, then simple dimensional analysis tells us that the smaller wedge should have the same dimensionless absorption coefficient  $A\left(\frac{\lambda}{\tau}\right)$  as the original. As shown in Fig. 6(b), this means that the cutoff frequency of the absorption will increase to 200 Hz, which loses the ability to measure sounds below 200 Hz—a crucial frequency range for many mechanical noises. However,

customized broadband metamaterial offers another possibility that can preserve the measurement capabilities in this frequency band. According to Eq. (1), if we want to keep the same working frequency range, half of the thickness will lead to a maximum absorption spectrum,  $A'$ , given by  $1 - A'(\lambda) \cong [1 - A(\lambda)]^{0.5}$ . Hence, the original absorption of  $A \sim 0.99$  becomes a stable absorption  $A' \sim 0.9$ . The photo in Fig. 6(a) shows an anechoic chamber with six sides entirely covered by metamaterial panels customized by following this idea. The relevant absorption spectrum is shown in Fig. 6(b), with an evident advantage below 150 Hz compared to the wedge sponge of the same thickness. In fact, the absorption [indicated by the red line in Fig. 6(b)] exceeds 0.9 above 85 Hz.

Customized absorption in a confined space can also adjust the reverberation time to create a comfortable acoustic environment. By customizing the absorption of the metamaterial wall, we can keep the reverberation time in a  $200 \times 100 \times 200 \text{ cm}^3$  confined space at a comfortable level ( $RT60 \sim 0.1 \text{ s}^{67}$ ) in the auditory-sensitive frequency band (200–8000 Hz). Such a space can provide the condition for clear and private telecommunication in the midst of a noisy environment.

## VI. CONCLUDING REMARKS

In this article, we show that the inherently narrow-frequency nature of the resonance-based acoustic metamaterial absorbers, traditionally regarded as the Achilles heel for applications, can become an advantage when integrated with the causal constraint in the realization of tunable absorbers. In spite of the challenges that still lie ahead, as well as the nontrivial task of mass customization, a paradigm shift is already under way in some sectors of airborne acoustics. From the history of R&D development, this can only mean the diversification of acoustic technologies, along with exciting prospects emerging on the horizon.

## ACKNOWLEDGMENTS

M.Y. and P.S. would like to thank Shuyu Chen for his support in realizing the goal of metamaterial absorber commercialization, and to Songwen Xiao, Caixing Fu, Yunfei Xu, and Mengyao Xie for their efforts in the projects described in this article. M.Y. would also like to thank Jack Oclee-Brown and Sebastien Degraeve for their cooperation in the loudspeaker project. P.S. would like to acknowledge AoE/P-502/20-3 for the support of open access charge of this article.

## AUTHOR DECLARATIONS

### Conflict of Interest

The authors have no conflicts to disclose.

### Author Contributions

**Min Yang:** Conceptualization (equal); Methodology (equal); Writing – original draft (equal); Writing – review & editing (equal). **Ping Sheng:** Conceptualization (equal); Methodology (equal); Writing – original draft (equal); Writing – review & editing (equal).

## DATA AVAILABILITY

The data that support the findings of this study are available within the article.

## REFERENCES

- Z. Liu, X. Zhang, Y. Mao, Y. Zhu, Z. Yang, C. T. Chan, and P. Sheng, “Locally resonant sonic materials,” *Science* **289**, 1734–1736 (2000).
- M. Yang, G. Ma, Z. Yang, and P. Sheng, “Coupled membranes with doubly negative mass density and bulk modulus,” *Phys. Rev. Lett.* **110**, 134301 (2013).
- Z. Liang and J. Li, “Extreme acoustic metamaterial by coiling up space,” *Phys. Rev. Lett.* **108**, 114301 (2012).
- J. Li, L. Fok, X. Yin, G. Bartal, and X. Zhang, “Experimental demonstration of an acoustic magnifying hyperlens,” *Nat. Mater.* **8**, 931–934 (2009).
- L. Zigoneanu, B.-I. Popa, and S. A. Cummer, “Three-dimensional broadband omnidirectional acoustic ground cloak,” *Nat. Mater.* **13**, 352–355 (2014).
- B. Liang, X. S. Guo, J. Tu, D. Zhang, and J. C. Cheng, “An acoustic rectifier,” *Nat. Mater.* **9**, 989–992 (2010).
- S. A. Cummer, J. Christensen, and A. Alù, “Controlling sound with acoustic metamaterials,” *Nat. Rev. Mater.* **1**, 16001 (2016).
- G. Ma and P. Sheng, “Acoustic metamaterials: From local resonances to broad horizons,” *Sci. Adv.* **2**, e1501595 (2016).
- M. Kadic, G. W. Milton, M. van Hecke, and M. Wegener, “3D metamaterials,” *Nat. Rev. Phys.* **1**, 198–210 (2019).
- Y. Wu, M. Yang, and P. Sheng, “Perspective: Acoustic metamaterials in transition,” *J. Appl. Phys.* **123**, 090901 (2018).
- X. Zhang, M. Xiao, Y. Cheng, M.-H. Lu, and J. Christensen, “Topological sound,” *Commun. Phys.* **1**, 97 (2018).
- G. Ma, M. Xiao, and C. T. Chan, “Topological phases in acoustic and mechanical systems,” *Nat. Rev. Phys.* **1**, 281–294 (2019).
- H. Xue, Y. Yang, and B. Zhang, “Topological acoustics,” *Nat. Rev. Mater.* **7**, 974–990 (2022).
- M. Yang and P. Sheng, “Sound absorption structures: From porous media to acoustic metamaterials,” *Annu. Rev. Mater. Res.* **47**, 83–114 (2017).
- J. Allard and N. Atalla, *Propagation of Sound in Porous Media: Modelling Sound Absorbing Materials*, 2nd ed. (John Wiley & Sons, 2009).
- G. Ma, M. Yang, S. Xiao, Z. Yang, and P. Sheng, “Acoustic metasurface with hybrid resonances,” *Nat. Mater.* **13**, 873–878 (2014).
- M. Yang, C. Meng, C. Fu, Y. Li, Z. Yang, and P. Sheng, “Subwavelength total acoustic absorption with degenerate resonators,” *Appl. Phys. Lett.* **107**, 104104 (2015).
- X. Cai, Q. Guo, G. Hu, and J. Yang, “Ultrathin low-frequency sound absorbing panels based on coplanar spiral tubes or coplanar Helmholtz resonators,” *Appl. Phys. Lett.* **105**, 121901 (2014).
- J. Li, W. Wang, Y. Xie, B.-I. Popa, and S. A. Cummer, “A sound absorbing metasurface with coupled resonators,” *Appl. Phys. Lett.* **109**, 091908 (2016).
- S. Kim, Y.-H. Kim, and J.-H. Jang, “A theoretical model to predict the low-frequency sound absorption of a Helmholtz resonator array,” *J. Acoust. Soc. Am.* **119**, 1933–1936 (2006).
- X. Wu, C. Fu, X. Li, Y. Meng, Y. Gao, J. Tian, L. Wang, Y. Huang, Z. Yang, and W. Wen, “Low-frequency tunable acoustic absorber based on split tube resonators,” *Appl. Phys. Lett.* **109**, 043501 (2016).
- N. Jiménez, W. Huang, V. Romero-García, V. Pagneux, and J. P. Groby, “Ultra-thin metamaterial for perfect and quasi-omnidirectional sound absorption,” *Appl. Phys. Lett.* **109**(12), 121902 (2016).
- V. Romero-García, G. Theocharis, O. Richoux, A. Merkel, V. Tournat, and V. Pagneux, “Perfect and broadband acoustic absorption by critically coupled sub-wavelength resonators,” *Sci. Rep.* **6**(1), 19519 (2016).
- N. Jiménez, V. Romero-García, V. Pagneux, and J. P. Groby, “Rainbow-trapping absorbers: Broadband, perfect and asymmetric sound absorption by sub-wavelength panels for transmission problems,” *Sci. Rep.* **7**(1), 13595 (2017).
- S. Huang, Z. Zhou, D. Li, T. Liu, X. Wang, J. Zhu, and Y. Li, “Compact broadband acoustic sink with coherently coupled weak resonances,” *Sci. Bull.* **65**(5), 373–379 (2020).
- V. Romero-García, N. Jiménez, J. P. Groby, A. Merkel, V. Tournat, G. Theocharis, O. Richoux, and V. Pagneux, “Perfect absorption in mirror-symmetric acoustic metascreens,” *Phys. Rev. Appl.* **14**(5), 054055 (2020).
- R. Dong, D. Mao, X. Wang, and Y. Li, “Ultrabroadband acoustic ventilation barriers via hybrid-functional metasurfaces,” *Phys. Rev. Appl.* **15**(2), 024044 (2021).
- M. Yang, S. Chen, C. Fu, and P. Sheng, “Optimal sound-absorbing structures,” *Mater. Horiz.* **4**, 673–680 (2017).

- <sup>29</sup>H. Long, Y. Cheng, and X. Liu, "Asymmetric absorber with multiband and broadband for low-frequency sound," *Appl. Phys. Lett.* **111**, 143502 (2017).
- <sup>30</sup>H. Chang, L. Liu, C. Zhang, and X. Hu, "Broadband high sound absorption from labyrinthine metasurfaces," *AIP Adv.* **8**, 045115 (2018).
- <sup>31</sup>X. Peng, J. Ji, and Y. Jing, "Composite honeycomb metasurface panel for broadband sound absorption," *J. Acoust. Soc. Am.* **144**, EL255–EL261 (2018).
- <sup>32</sup>X.-F. Zhu, S.-K. Lau, Z. Lu, and W. Jeon, "Broadband low-frequency sound absorption by periodic metamaterial resonators embedded in a porous layer," *J. Sound Vib.* **461**, 114922 (2019).
- <sup>33</sup>H. Long, C. Shao, C. Liu, Y. Cheng, and X. Liu, "Broadband near-perfect absorption of low-frequency sound by subwavelength metasurface," *Appl. Phys. Lett.* **115**, 103503 (2019).
- <sup>34</sup>C. R. Liu, J. H. Wu, X. Chen, and F. Ma, "A thin low-frequency broadband metasurface with multi-order sound absorption," *J. Phys. D* **52**, 105302 (2019).
- <sup>35</sup>H. Long, C. Liu, C. Shao, Y. Cheng, K. Chen, X. Qiu, and X. Liu, "Subwavelength broadband sound absorber based on a composite metasurface," *Sci. Rep.* **10**, 13823 (2020).
- <sup>36</sup>Y.-X. Gao, Y.-P. Lin, Y.-F. Zhu, B. Liang, J. Yang, J. Yang, and J.-C. Cheng, "Broadband thin sound absorber based on hybrid labyrinthine metastructures with optimally designed parameters," *Sci. Rep.* **10**, 10705 (2020).
- <sup>37</sup>J. Guo, Y. Fang, Z. Jiang, and X. Zhang, "Acoustic characterizations of Helmholtz resonators with extended necks and their checkerboard combination for sound absorption," *J. Phys. D* **53**, 505504 (2020).
- <sup>38</sup>J. Boulvert, J. Costa-Baptista, T. Cavaliere, V. Romero-García, G. Gabard, E. R. Fotsing, A. Ross, M. Perna, J. Mardjono, and J.-P. Groby, "Folded metaporous material for subwavelength and broadband perfect sound absorption," *Appl. Phys. Lett.* **117**, 251902 (2020).
- <sup>39</sup>H. Long, C. Liu, C. Shao, Y. Cheng, J. Tao, X. Qiu, and X. Liu, "Tunable and broadband asymmetric sound absorptions with coupling of acoustic bright and dark modes," *J. Sound Vib.* **479**, 115371 (2020).
- <sup>40</sup>H. Nguyen, Q. Wu, X. Xu, H. Chen, S. Tracy, and G. Huang, "Broadband acoustic silencer with ventilation based on slit-type Helmholtz resonators," *Appl. Phys. Lett.* **117**, 134103 (2020).
- <sup>41</sup>S. Kumar and H. P. Lee, "Labyrinthine acoustic metastructures enabling broadband sound absorption and ventilation," *Appl. Phys. Lett.* **116**, 134103 (2020).
- <sup>42</sup>X. Xiang, X. Wu, X. Li, P. Wu, H. He, Q. Mu, S. Wang, Y. Huang, and W. Wen, "Ultra-open ventilated metamaterial absorbers for sound-silencing applications in environment with free air flows," *Extreme Mech. Lett.* **39**, 100786 (2020).
- <sup>43</sup>N. Gao, D. Luo, B. Cheng, and H. Hou, "Teaching-learning-based optimization of a composite metastructure in the 0–10 kHz broadband sound absorption range," *J. Acoust. Soc. Am.* **148**, EL125–EL129 (2020).
- <sup>44</sup>Z.-X. Xu, H.-Y. Meng, A. Chen, J. Yang, B. Liang, and J.-C. Cheng, "Tunable low-frequency and broadband acoustic metamaterial absorber," *J. Appl. Phys.* **129**, 094502 (2021).
- <sup>45</sup>J. Guo, X. Zhang, Y. Fang, and Z. Jiang, "Wideband low-frequency sound absorption by inhomogeneous multi-layer resonators with extended necks," *Compos. Struct.* **260**, 113538 (2021).
- <sup>46</sup>H. Long, C. Shao, Y. Cheng, J. Tao, and X. Liu, "High absorption asymmetry enabled by a deep-subwavelength ventilated sound absorber," *Appl. Phys. Lett.* **118**, 263502 (2021).
- <sup>47</sup>J. Guo, Y. Fang, R. Qu, Q. Liu, and X. Zhang, "An extra-broadband compact sound-absorbing structure composing of double-layer resonator with multiple perforations," *J. Acoust. Soc. Am.* **150**, 1370–1380 (2021).
- <sup>48</sup>T. Cavaliere, J. Boulvert, V. Romero-García, G. Gabard, M. Escoufflaire, J. Regnard, and J.-P. Groby, "Rapid additive manufacturing of optimized anisotropic metaporous surfaces for broadband absorption," *J. Appl. Phys.* **129**, 115102 (2021).
- <sup>49</sup>Y. Zhu, A. Merkel, K. Donda, S. Fan, L. Cao, and B. Assouar, "Nonlocal acoustic metasurface for ultrabroadband sound absorption," *Phys. Rev. B* **103**, 064102 (2021).
- <sup>50</sup>Z. Wang, Z. Guo, Z. Li, and K. Zeng, "Coupling and scaling effect for low-frequency broadband sound absorption via vertex-based hierarchy," *Appl. Phys. Lett.* **119**, 171903 (2021).
- <sup>51</sup>Z. Zhou, S. Huang, D. Li, J. Zhu, and Y. Li, "Broadband impedance modulation via non-local acoustic metamaterials," *Natl. Sci. Rev.* **9**, nwab171 (2022).
- <sup>52</sup>Y. Jin, Y. Yang, Z. Wen, L. He, Y. Cang, B. Yang, B. Djafari-Rouhani, Y. Li, and Y. Li, "Lightweight sound-absorbing metastructures with perforated fish-belly panels," *Int. J. Mech. Sci.* **226**, 107396 (2022).
- <sup>53</sup>A. Chen, Z.-X. Xu, B. Zheng, J. Yang, B. Liang, and J.-C. Cheng, "Machine learning-assisted low-frequency and broadband sound absorber with coherently coupled weak resonances," *Appl. Phys. Lett.* **120**, 033501 (2022).
- <sup>54</sup>H. Ryoo and W. Jeon, "Broadband sound absorption using multiple hybrid resonances of acoustic metasurfaces," *Int. J. Mech. Sci.* **229**, 107508 (2022).
- <sup>55</sup>L. Liu, L.-X. Xie, W. Huang, X. J. Zhang, M.-H. Lu, and Y.-F. Chen, "Broadband acoustic absorbing metamaterial via deep learning approach," *Appl. Phys. Lett.* **120**, 251701 (2022).
- <sup>56</sup>C. Shao, Y. Zhu, H. Long, C. Liu, Y. Cheng, and X. Liu, "Metasurface absorber for ultra-broadband sound via over-damped modes coupling," *Appl. Phys. Lett.* **120**, 083504 (2022).
- <sup>57</sup>Z. Li, X. Li, Z. Wang, and W. Zhai, "Multifunctional sound-absorbing and mechanical metamaterials via a decoupled mechanism design approach," *Mater. Horiz.* **10**, 75 (2023).
- <sup>58</sup>J. D. Jackson, *Classical Electrodynamics*, 3rd ed. (John Wiley & Sons, New York, 1999).
- <sup>59</sup>H. W. Bode, *Network Analysis and Feedback Amplifier Design* (van Nostrand, New York, 1945).
- <sup>60</sup>R. M. Fano, "Theoretical limitations on the broadband matching of arbitrary impedances," *J. Franklin Inst.* **249**, 57–83 (1950).
- <sup>61</sup>K. N. Rozanov, "Ultimate thickness to bandwidth ratio of radar absorbers," *IEEE Trans. Antennas Propag.* **48**, 1230–1234 (2000).
- <sup>62</sup>O. Acher, J. Bernard, P. Maréchal, A. Bardaine, and F. Levassort, "Fundamental constraints on the performance of broadband ultrasonic matching structures and absorbers," *J. Acoust. Soc. Am.* **125**, 1995–2005 (2009).
- <sup>63</sup>H. W. Kuhn and A. W. Tucker, "Nonlinear programming," in *Traces and Emergence of Nonlinear Programming* (Springer, 2013), pp. 247–258.
- <sup>64</sup>J. Fan, L. Zhang, S. Wei, Z. Zhang, S.-K. Choi, B. Song, and Y. Shi, "A review of additive manufacturing of metamaterials and developing trends," *Mater. Today* **50**, 303–328 (2021).
- <sup>65</sup>C. Choi, S. Bansal, N. Münzenrieder, and S. Subramanian, "Fabricating and assembling acoustic metamaterials and phononic crystals," *Adv. Eng. Mater.* **23**, 2000988 (2021).
- <sup>66</sup>S. Degraeve and J. Oclec-Brown, "Metamaterial absorber for loudspeaker enclosures," in *Audio Engineering Society Convention 148* (Audio Engineering Society, 2020).
- <sup>67</sup>F. A. Everest and K. C. Pohlmann, *Master Handbook of Acoustics*, 6th ed. (McGraw-Hill Education, New York, 2022).